Bibliography

[1] DIMITRIADIS, G. **Experimental aerodynamics lecture 5: Experimental characteristics of wings sections**.

[2] SCHLICHTING, H. **Boundary Layer Theory**. 7th. ed., McGraw-Hill, 1979.

[3] PATANKAR, S. V. **Numerical Heat Transfer and Fluid Flow**. Hemisphere Publishin Corporation, 1980.

[4] WILCOX, D. C. **Turbulence Modeling for CFD**. DCW Industries, July 1993.

[5] MENTER, F. Two-equation eddy-viscosity turbulence models for engineering applications. **AIAA Journal**, v.32, n.8, p. 1598–1605, August 1994.

[6] JAMESON, A.; MARINELLI, L. Mesh refinement and modeling errors in flow simulation. **AIAA**, 1996.

[7] JASAK, H. **Error analysis and estimation for the finite volume method whit applications to fluid flows**. June 1996. PhD thesis, Imperial College.

[8] SAWLEY, M. L.; RICHTER, R. nov 1997. Technical Report 9.

[9] GODIN, P.; ZINGG, D. W. High-lift aerodynamic computations with one- and two-equation turbulence models. **AIAA**, v.35, n.2, p. 237–143, February 1997.

[10] SELING, M.; GUGLIELMO, J. J. High-lift low reynolds number airfoil design. **Journal of Aircraft**, v.34, n.1, p. 72–79, January-February 1997.

[11] MEHTA, U. B. Credible computational fluid dynamics simulation. **AIAA**, v.36, n.5, May 1998.

[12] HABASHI, W. G. Certifiable computational fluid dynamics through mesh optimization. **AIAA**, v.36, n.5, p. 703–711, May 1998.

[13] AIAA. **Guide for the verification and validation of computational fluid dynamics simulations**. American Institute of Aeronautics and Astronautics, Jan. 1998. Technical Report G-077-1998.

[14] RAMESH, A. Computational fluid dynamics of a whole-body aircraft. **Annu. Rev. Fluid Mechanics**, n.1999. 31:125–69, p. 126–169, 1999.

[15] POPE, S. B. **Turbulent Flows**. Cambridge University Press, 2000.

[16] OPENCFD. **Openfoam features**, 2001.

[17] ANDERSON, J. J. D. **Fundamentals of Aerodynamics**. 3rd. ed., New York: McGraw-Hill, 2001.

[18] SIMPSON, R. L. Junction flows. **Annu. Rev. Fluid Mechanics**, v.33, p. 415–443, January 2001.

[19] SOSO, M.; SELING, M. An angle of attact correction scheme for the desing of low aspect ratio wings with end plates. **SAE**, n.2002-01-3292, December 2002.

[20] GERRISTMA, M. I. **Computational fluid dynamics: Incompressible flows**. July 2002.

[21] ZHANG, X.; ZERIHAN, J.; RUHRMANN, A.; DEVIESE, M. ; OTHERS. Tip vortice generated by a wing in ground effect. **Proceedings of the 11th International Symposium on Applications of Laser Techniques to Fluid Mechanics**, 2002.

[22] MYES, B. B. **Experimental and numerical studies of the effects of upper surface roughness on aileron performance**. Council, Canada National Research, 2003. Technical report.

[23] BIENZ, C.; LARSSON, T. ; ULLBRAND, B. In front of the grid - cfd at sauber petronas f1 leading the aerodynamic development. **1st European Automotive CFD Conference**, June 2003.

[24] LUCKRING, J. M.; HEMSCH, M. J. ; MORIISON, J. H. Uncertainty in computational aerodynamics. **AIAA**, n.0409, January 2003.

[25] MENTER, F.; KUNTZ, M. ; LANGTRY, R. Ten years of industrial experience with sst turbulence model. **Turbulence , Head and Mass Transfer 4**, v.4, 2003.

[26] BRABDT, L.; SCHLATTER, P. ; HENNINGSON, D. S. Transition in boundary layers subjected to free-stream turbulence. **Journal of Fluid Mechanics**, v.517, n.517, p. 167–198, 2004.

[27] LARSSON, T.; SATO, T. ; ULLBRAND, B. **F1 supercomputing: Unlocking the power of cfd**. SAUBER PETRONAS Engineering AG, 2005. Technical report.

[28] KATZ, J. **Race Car Aerodynamics: Designing for Speed**. 2nd. ed., Cambridge: Bently Publishers, 2006.

[29] SAMPAIO, L. E. **Simulação de Grandes Escalas da Bolha de Separação en Placas Finas a Pequeno Ângulo de Incidência**. September 2006. PhD thesis, PUC-Rio.

[30] SOSO, M.; WILSON, P. Aerodynamics of a wing in ground effect in generic racing car wake. **Journal of Automobile Engineering**, v.220, n.1, p. 1–13, 2006.

[31] TORRES-NIEVES, S. N. **Turbulent boundary layers: Free stream turbulence, sourface roughness, ans favorable pressure gradient**. Troy, New York, Aug. 2007. Master's thesis, Rensselaer Polytechnic Institute.

[32] SCHWER, L. E.; OBERKAMPF, W. L. Special issue on verification and validation. **Engineering with Computers**, n.23, p. 243–244, June 2007.

[33] WÖTHRICH, B. **Simulation and validation of compressible flow in nozzle geometries and validation of openfoam for this application**. 2007. Master's thesis, Institute of Fluid Dynamics ETH Zurich.

[34] HIRSCH, C. **Fundamentals of Computational Fluid Dynamics**, volume 1 of **Numerical Computation of Internal and External FLows**. 2nd. ed., Butterworth-Heinemann, 2007.

[35] GALUOL, V.; BARBER, T. A study of an inverted wing with endplates in ground effect. **Australian Fluid Mechanics Conference** 16^{th}, December 2007.

[36] GENUA, E. **A cfd investigation into ground effect aerodynamics**. July 2009. Master's thesis, Delft University of Technology.

[37] WENT, J. F. **Computational Fluid Dynamics an Introduction**. Third. ed., Springer, 2009.

A
Airfoil Data

x	y	x	y	x	y
0	0	111.7223	11.5498	100.4406	-12.8232
0.2234	1.7649	122.8923	11.3711	89.2706	-14.0965
0.4468	2.4351	134.0623	11.0806	78.1006	-15.1689
1.1393	3.8648	145.21	10.7009	66.9306	-16.1071
2.2563	5.1829	156.38	10.187	55.7606	-16.822
3.3733	6.0318	167.55	9.5839	44.5906	-17.2241
4.4903	6.6797	178.72	9.1371	40.1226	-17.0454
5.6073	6.9701	189.89	9.2041	35.6546	-16.621
6.7243	7.1711	201.06	9.9636	31.1866	-15.9284
7.8413	7.3499	205.528	10.4551	26.741	-15.0125
8.9583	7.5062	209.996	11.0806	22.273	-13.8285
10.0753	7.685	214.464	11.7732	20.039	-13.1359
11.1923	7.8637	218.932	12.5774	17.805	-12.3764
12.3093	8.0201	221.166	13.0242	15.5933	-11.5721
13.4263	8.1988	223.4	13.471	13.3593	-10.7009
15.6603	8.4669	221.166	12.8008	12.2423	-10.2317
17.8943	8.7573	218.9097	12.1306	11.1253	-9.7402
20.1507	9.0254	214.4417	10.8126	10.0083	-9.2488
22.3847	9.2264	209.9737	9.5168	8.8913	-8.7573
26.8527	9.6509	205.5057	8.2658	7.7743	-8.2211
31.3207	9.9636	201.0377	7.0371	6.6573	-7.685
35.7887	10.2094	189.8453	4.0882	5.5627	-7.1265
40.2567	10.3881	178.6753	1.3404	4.4457	-6.5456
44.7247	10.5668	167.5053	-1.251	3.3287	-5.9424
55.8723	10.9243	156.313	-3.6414	2.2117	-5.0935
67.0423	11.2594	145.143	-5.8307	1.0947	-3.7531
78.2123	11.4828	133.973	-7.8413	0.4468	-2.3904
89.3823	11.5945	122.803	-9.6956	0.2234	-1.6978
100.5523	11.6391	111.6106	-11.3487	0	0

Table A.1: Coordinates listing of the Tyrrel airfoil

B
Paper

In this appendix is presented the paper sent to the Iberian Latin American Congress on Computational Methods in Engineering (CILAMCE).

NUMERICAL SIMULATION OF THE FLOW AROUND THE REAR WING OF A RACING CAR

L. Daniel Peralta M.[a], **Sergio Leal Braga**[a] **and Luiz E. B. Sampaio**[b]

[a]*Department of Mechanical Engineering — PUC–Rio, http://www.mec.puc-rio.br/*

[b]*Laboratory of Theoretical and Applied Mechanics LMTA/PGMEC – UFF, http://www.lmta.mec.uff.br/*

Keywords: Computational Fluid Dynamics, Wing, Aerodynamics, Racecar.

Abstract. In a tentative to reduce the time and cost of aerodynamic simulations, the preset study uses a free open-source code (OpenFOAM) to assess the flow around the rear wing of a race car, in particular, the PUC-Rio Formula-University car. To diminish the time it takes to prepare a numerical simulation, we evaluate the suitability and accuracy of a particular utility available in OpenFOAM, namely, snappyHexMesh. The effect of using such a grid in numerical simulations employing two different turbulence models for several angles of attack is investigated. The numerical simulation comprised six steps: 3D scanning, geometry modeling, grid generation, flow computation, solution validation, flow visualization and analysis. The results obtained in the validation process showed that two-dimensional simulations ran onto the unstructured grid agreed with experimental data, presenting a difference in the lift coefficient ranging between 3% and 8%. While comparing the results with numerical validated data the difference ranged between 0.5% and 3.6%. The simulation of the flow around the rear wing showed that this methodology is capable to capture the essential physics of three-dimensional external flow. Consequently, thanks to the advantages and accuracy described in the preset study, this method is considered to be able to diminish the total time of a simulation and therefore its global cost.

1 INTRODUCTION

Nowadays in the world of the motorsport industry, among the several research fields involved in the design of race cars, aerodynamics is the most rewarding in terms of performance improvements per resource and time invested. Engineers found that using aerodynamic devices to generate negative lift enhances the overall car performance, decreasing lap times. This extra force helps to vary notably the dynamic behavior of the car enabling faster cornering speeds as well as shorter breaking lengths.

Wings have been an important part in the complex aerodynamic arrangement that involves a racing car since its appearance in motorsport. Wings aerodynamics has been studied exhaustively by experimental methods. However, currently this technique is complemented by numerical techniques which, thanks to the incredible development of computational power along with new discretization schemes to be used with unstructured grids, has become a fundamental tool to optimize the wings performance by studying the different factors that influence the flow around them.

Previous studies have shown the advantages of using numerical techniques to assess the flow around aerodynamic devices. Larsson et al. (2005), show that using unstructured grids facilitates the grid generation process of large and complex assemblies, demonstrating that using hexahedral elements can produce results with lower numerical diffusion than those using tetrahedral elements, as well as lower number of elements. Bienz et al. (2003), demonstrate the utility of CFD in the design and optimization processes of new racing car components including the front and rear wings. Seibert and Lewis (2004), show the developments in the application of unstructured grids to solve different type of problems in motorsport such as the influence of wings wake in overtaking maneuvers.

An important factor that has allowed the acceptance of CFD in the aerodynamic design process is the detailed validation work which it has been subjected to. Paradoxically, the validation process requires experimental data to test the suitability and accuracy of the simulations to describe a particular phenomenon. For this reason, numerous experimental studies are still being carried out in order to gain deeper understanding of complex flow phenomena and contribute to increase information sources to validate numerical models. In the area of race car wings, for instance, Zhang et al. (2002), studied the tips vortices generated by a cambered, single-element wing operating in ground effect, using particle image velocity along with laser Doppler anemometry and some visualization techniques. In this study the downforce was found affected by the presence of separation on the suction surface and the wing tip vortex. Tip vortex induced an upwash on the wing, leading to an effective reduction in the incidence of the wing and hence smaller extents of separation near the wing. A similar study was carried out by Galuol and Barber (2007), in which the aerodynamics of an inverted wing with end plates in ground effect was investigated, using laser Doppler anemometry to measure the flow field near the trailing edge and smoke to visualize the flow around the tips. The results showed the formation of two corotating vortices originating from the top and the bottom of the end plate. Also, it was identify that both vortices interact with each other. The stronger vortex alters the trajectory of the weaker one, and merges with it downstream. On the other hand, **?**, presented a more complete study, showing the influence of some elementary factors in the flow around an inverted, two-element wing configuration in and out of ground effect. The results showed that parameters such as the Reynolds number, angles of attack, end plate design, among others, have a significant effect on the wing performance. Furthermore, flow flied measurements in some planes near the trailing edge showed the formation of two large trailing vortices rolling up from the end plates edges, as well as a smaller forming from the junction of the end plate and the wing.

Although the aforementioned studies are concerned specifically to the analysis of the influence of the ground effect in the downforce and the overall flow, some authors such as Galuol and Barber (2007), **?**, clearly show that the influence of the ground effect in the flow field structures is only appreciable in ground/wing clearances lower than 10%. Therefore, the previously mentioned description of the flow structures is also applicable to out of ground wing setups.

2 PRESENT STUDY

Two major stages, influencing the total time and cost of numerical simulations, are those related to grid generation and processing time. Optimizing at least one of them would result in a considerable reduction of the simulation time and cost. To this purpose, automatic grid generators appear as a viable alternative, since they are cable to deal with complex geometries and produce relatively less elements than those produced by traditional methods.

Therefore, the present study is aimed at validating and assessing an automatic 3D mesh generation method through the solution and analysis of a real problem. This problem consist in the simulation of the flow around the rear wing of the Formula Student car owned by PUC-Rio. The analysis will be carry out visualizing the flow and judging if the results correspond to real physical conditions. Focusing to decrease the overall cost of the simulation, it is proposed to employ an open-source code so as to generate the grid and solve the simulation.

3 COMPUTATIONAL MODELING

The current study is done using the OpenFOAM open-source code. The discretization method implemented in the code is a Finite Element Method for structured and unstructured grids. The incompressible steady-state solver simpleFoam along with Upwind schemes were used to solve the three dimensional Reynolds Average Navier-Stokes equations. The Spalart Allmaras and $k-\omega SST$ models were used to close the system of equations.

$$\frac{\partial \bar{u}_i}{\partial x_i} = 0 \ , \tag{1}$$

$$\bar{u}_j \frac{\partial \bar{u}_i}{\partial x_j} = -\frac{1}{\rho}\frac{\partial \bar{p}}{\partial x_i} + \nu \frac{\partial^2 \bar{u}_i}{\partial x_j \partial x_j} - \frac{\partial \overline{u_i' u_j'}}{\partial x_j} \ , \tag{2}$$

where u_i is the ith component of the velocity vector, p is the static pressure, ρ is the air density, ν is the kinematic air viscosity, and $\overline{u_i' u_j'}$ is the Reynolds stress tensor modeled by the turbulence models mentioned above.

The convergence criterion is based on the residuals of the governing equations and the aerodynamic coefficients. When the residual were as low as 10^{-7} and the lift and drag coefficients were observed to reach steady state values, simulations were stopped.

3.1 Grid Generation

The tool used to get the domain discretized is the automatic mesh-generator utility supplied by OpenFOAM, named snappyHexMesh. This utility generates three-dimensional unstructured grids automatically, containing hexahedra and split-hexahedra, from a triangulated surface geometry in Stereolithography (STL) format. The grid generation process consist of five steps. First, it begins creating a hexahedral box covering the entire computational domain. Second, this box is split into equal smaller hexahedral cells covering even the solid geometry. Third, the hexahedral cells are split again but only around the geometry surface as many times as defined in the grid controls. Fourth, the cells inside the geometry are removed. Fifth, to remove the jagged surface that remains around the geometry from the later stage, the vertex points inside the geometry are snapped to its surface to contour its outline. Sixth, layers of hexahedral cells are added to the geometry surface to represent the boundary layer over it.

4 GRID STUDY

A grid study was carried out with the aim at clarifying the effect of grid refinement on the aerodynamic force and evaluate the behavior of two turbulence models in grids with different refinement near the wall. The study consisted in simulating the flow around the Tyrell026 airfoil under the same flow and boundary conditions published in the report of Genua (2009). Thus, the results could be validated comparing them with the experimental and numerical results presented in the aforementioned report.

The results showed a good agreement with the experimental data, presenting a difference in the lift coefficient ranging between 3% and 8%. This variation indicates a large dependence on the grid refinement, specially in the chordwise refinement of the near-wall layers. Regarding the influence of the first elements height, there is a clear discrepancy in the results when the grid is closer to the wall, due to the different approaches used by each wall function to solve the flow near the walls.

While comparing the results with the numerical data the difference ranged between 0.5% and 3.6%, showing the same same tendency, overpredicting the lift coefficient when low aspect ratio cells are used near the wall. The $k - \omega SST$ model gave better results in the finer grids, while the Spalart Allmaras model gave a good result in the coarse grid and not much consistent results in the finer grids. A more complete description of the validation process is presented in Peralta (2011).

5 REAR WING SIMULATION

5.1 Test case description

The geometry employed in the three-dimensional simulations was the rear wing of the PUC-Rio Formula Student car. It is a rectangular inverted wing with a total span of 1.125 $[m]$, with end plates at the tips. The single-element airfoil comprising the rear wing cross-section is a high cambered airfoil with a cord length of 0.19 $[m]$.

5.2 Computational Domain

The computational domain, shown in Fig. [1], consists of six external patches (inlet, outlet, back, front, bottom, top) and an internal one (rearWing). A refinement box is placed inside the domain where the majority of cells are concentrated. The wing is place at 1 $[m]$ above the bottom plane and the angle of attack is changed rotating the wing geometry before the grid generation. A half of the domain is considered with a vertical symmetric plane defined at the wing mid span to save the computation time. To illustrate the resulting grid, Fig. [1] shows an example of a grid layout.

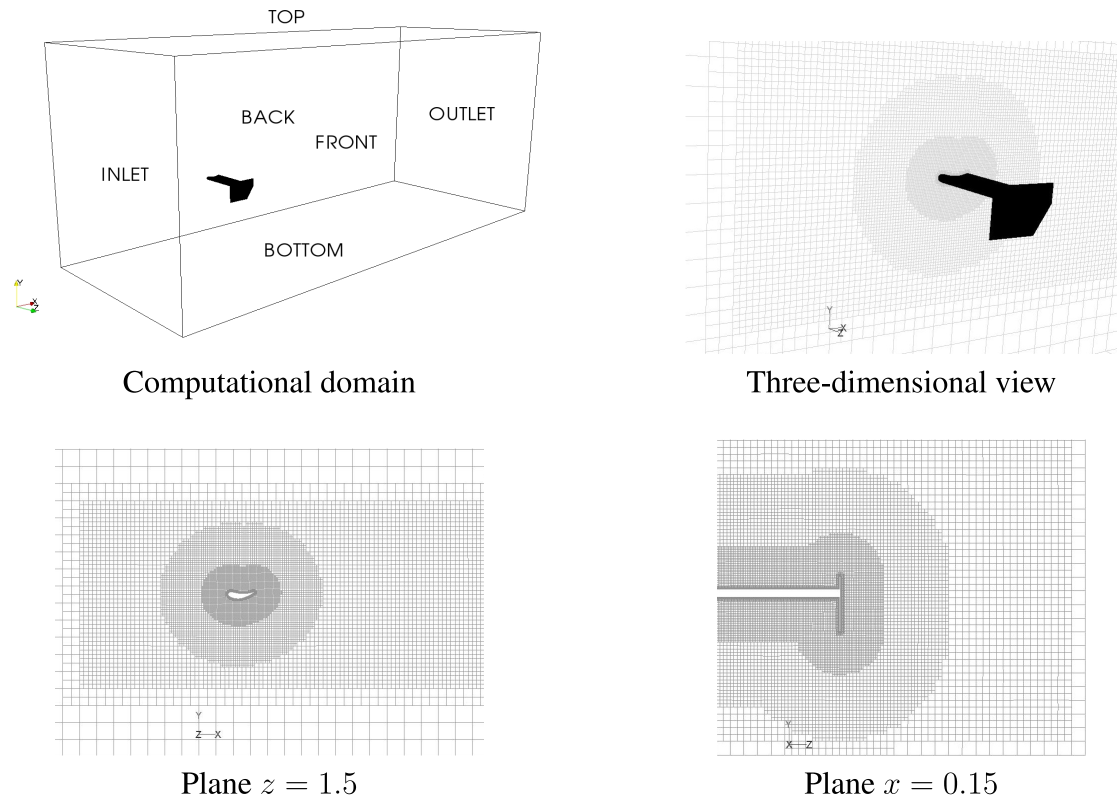

Figure 1: Example of the cells distribution on Grid M10

5.3 Boundary Conditions

Non-slip boundary conditions are applied on the wing, top, and front surfaces. Symmetry boundary condition is applied on the back surface. Fixed velocity is applied on the inlet surface. Outflow boundary condition is applied on the outlet surface.

Average conditions of velocity and turbulence were considered to set the boundary conditions. A constant value of 120 $[km/h]$ (33.3 $[m/s]$) in the x direction was set as inlet velocity. This value corresponds to an average velocity selected according to the expected performance of the formula car. As a result, the Reynolds number based on the free-stream velocity and the chord length is 4.2×10^5.

The free-stream turbulence intensity was tested to evaluate its influence in the simulation results. Two typical values for wind tunnel experiments were employed (0.3% and 1%), which did not affected significantly the computed velocity field.

6 RESULTS

The analysis and discussion of the results is divided in two parts. First, the grids are assessed. Second, the results are analyzed for two angles of attack, based on the pressure distribution and flow visualization.

The y^+ values around the wing are used as a first criterion in the assessment of the grid. Contours of y^+ for $0°$ and $15°$ of incidence are presented in Fig. [2]. They show a very high value (blue zones) where the mesh near-wall layers were incorrectly generated or were not generated at all. In the case of the end plate tips, mostly for $15°$ of incidence, the blue zones does not correspond to flaws in the grid, but to separation zones.

The y^+ values are high at the stagnations points, since at that locations the boundary layer is inexistent or rather small. Afterwards, they decrease along the chord at the upper surface, since the thickness of the boundary layer increases and the first layer of nodes remains at the same position. On the suction surface they decrease along the chordwise, showing that the boundary layer thickness decreases due to the higher velocity under the wing. As a matter of fact, the higher values of y^+ corresponds to separation zones found in the suction surface, and around the end plate tips in the case of $15°$ of incidence.

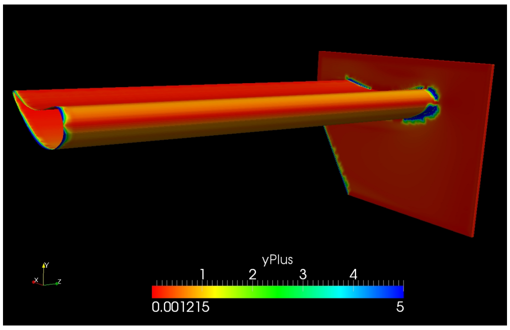

$k - \omega SST$ $0°$ Front view

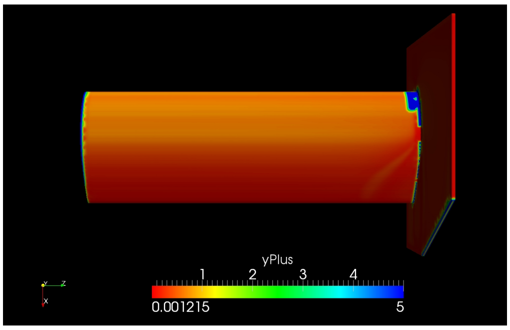

$k - \omega SST$ $0°$ Wing lower surface

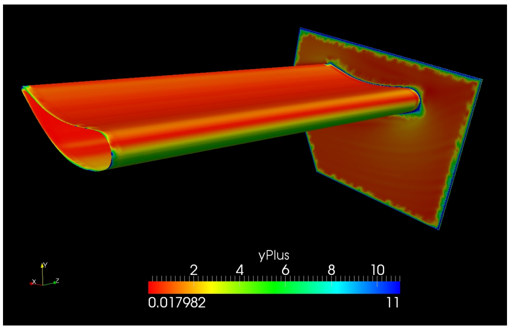

$k - \omega SST$ $15°$ Front view

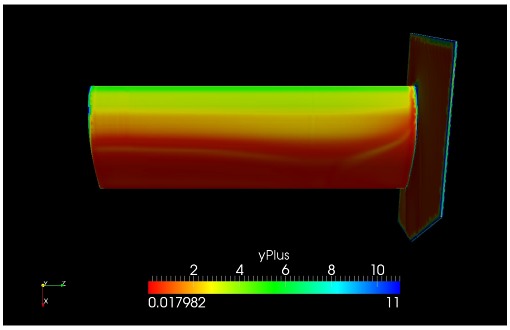

$k - \omega SST$ $15°$ Wing lower surface

Figure 2: Distribution of y^+ values on the wing surface

6.1 Aerodynamic Coefficients

Six different grids were created setting up six different sets of refinement parameters. The resulting features of the six grids are shown in table [1]. Two of these six grids do not have near-wall layers [M0, M1].

Grid	N. of Cells	non-Orthogonality	Max. Skewness
M0	1065328	26.97	0.85
M1	2045619	26.27	1.08
M10	1862173	64.55	1.29
M15	1643133	57.92	2.23
M20	2014783	54.80	2.49
M21	7928824	64.89	1.88

Table 1: Grid features

Figure [3] shows the results of the lift coefficient C_L for the $k-\omega SST$ model. Comparing the results of each grid, it is clear that using grids whose cells near the wall have low aspect ratios (grids [M0, M1] and [M20]), the results of C_L are larger than those predicted with the grids using high aspect ratio cells near the wall (grids [M10, M15] and [M21]).

From these results it is possible to conclude that the use of near-wall layers affects largely the predicted values of lift coefficients. According to Went (2009), the discrepancy in the results previously mentioned can be explained, since the alignment of the grid with the flow provided by the near wall layers leads to less numerical diffusion in the streamlines direction. In fact, if these aligned cell layers have a high aspect ratio, numerical diffusion can be further reduced.

Also, It can be noticed from this figure that the results are quite sensitive to the first layer height. Comparing [M10, M20, M21] with [M15], it is obvious that the location of the first nodes affected the manner that the turbulence model solved the flow near the wall.

The results of the lift coefficient predicted by the Spalart Allmaras model are presented in Fig. [4]. In this case, the results follow the same growing trend as those in the previous figure. Lift coefficients are larger in the [M0] and [M1] grids and accordingly to what was found in the two-dimensional validation the coarsest grid, [M15], also predicted larger values of lift compared with the finer grids.

The difference among the finer three grids [M10, M20, M21] is smaller having almost the same values for all the angles of attack. Compared to the previous model, the Spalart Allmaras predicted larger values of C_L in the coarser grids [M0, M1]. Comparing both models in Fig. [5], one can notice that the Spalart Allmaras model is more sensitive to the near-wall grid refinement than the $k-\omega SST$ model. Furthermore, the values predicted by this model in the finer grids are lower than those predicted by the $k-\omega\ SST$. This difference is considerable and grows as the angle of attack grows. This is due the fact that each turbulence model computes turbulence in a different manner, which results in significant disagreement in the prediction of separation. Finally, comparing the finer grids [M10, M21], it can be noted that they present similar results, which suggests grid convergence.

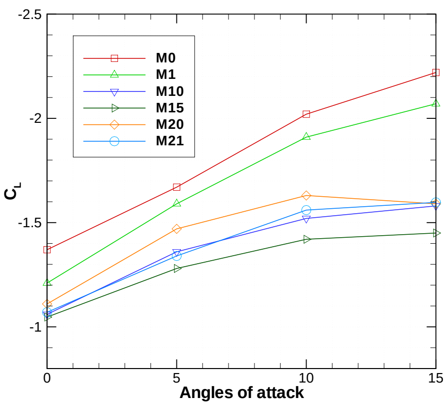

Figure 3: C_L results using $k-\omega\ SST$ model

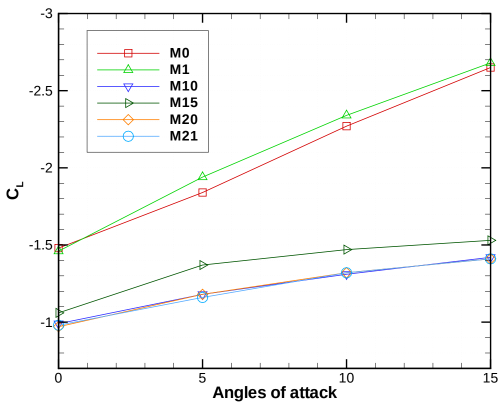

Figure 4: C_L results using Spalart Allmaras model

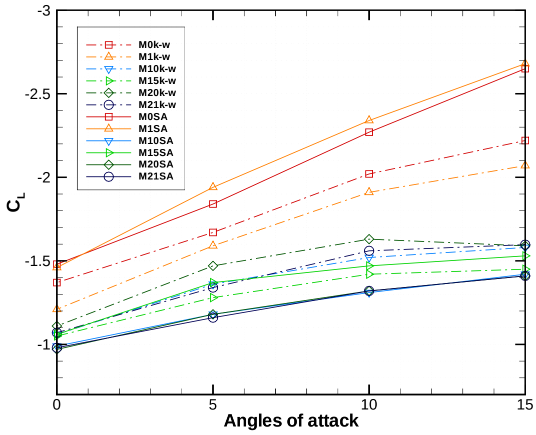

Figure 5: Comparison of the lift coefficient for the two turbulence models

Figures [6] and [7] present the results for the drag coefficient and for each turbulence models, respectively. There is not much differences among the predicted values for the finer grids, and all the grids share the same growing trend with similar curve slopes. As expected, the growing trend confirms that the drag coefficient increases as the angle of attack increases. Similar to the lift coefficient, the discrepancy among the results grows with the angle of attack due to different level in the prediction of separation. Furthermore, it is interesting to note that the grid refinement affects in a grater manner the prediction of drag in aerodynamic flows. This is due to the fact that not only the near-wall refinement is important to calculate the drag, but also the near velocity field affecting the pressure around the wing. In other words, since the drag is the resultant of three different effects (skin friction, pressure drag and induced drag), its accurate prediction depends on the grid being able to capture all the physics of the flow, namely, friction at walls, separation, and tip vortex structures effects.

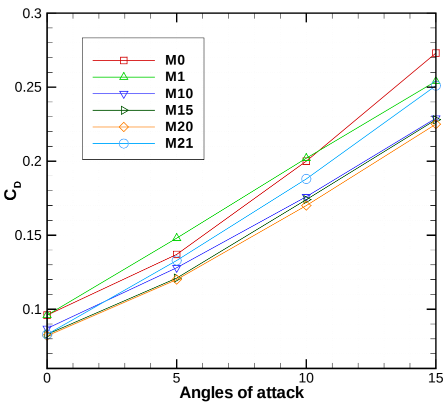

Figure 6: C_D results using $k - \omega SST$ model

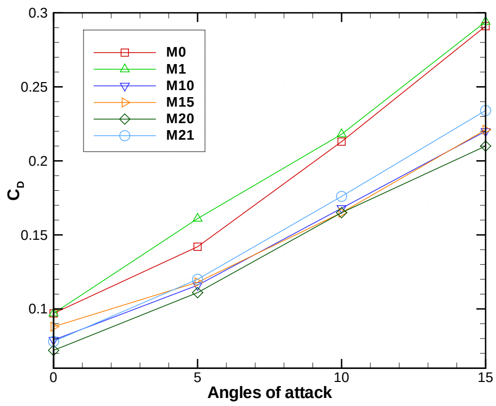

Figure 7: C_D results using Spalart Allmaras

6.2 Pressure Distribution

Figure [8] shows the three-dimensional pressure contours over the surface of the rear wing for $0°$ of incidence. In this figure, both turbulence models predict similar pressure distributions, with a slight difference in the minimum pressure value. The contour shows the highest pressure at the stagnation zone. At the upper surface, there two areas of low pressure produced by the excessive curvature near the leading edge and the trailing edge. The suction surface is characterize by a red area where the minimum pressure is attained, followed by an increase in the pressure until the trailing edge. It is important to note that the pressure field in this surface is affected by the proximity of the wing tip. It seems that such alteration is due to the influence of the tip vortex originated by the strong pressure difference between the upper and lower surface.

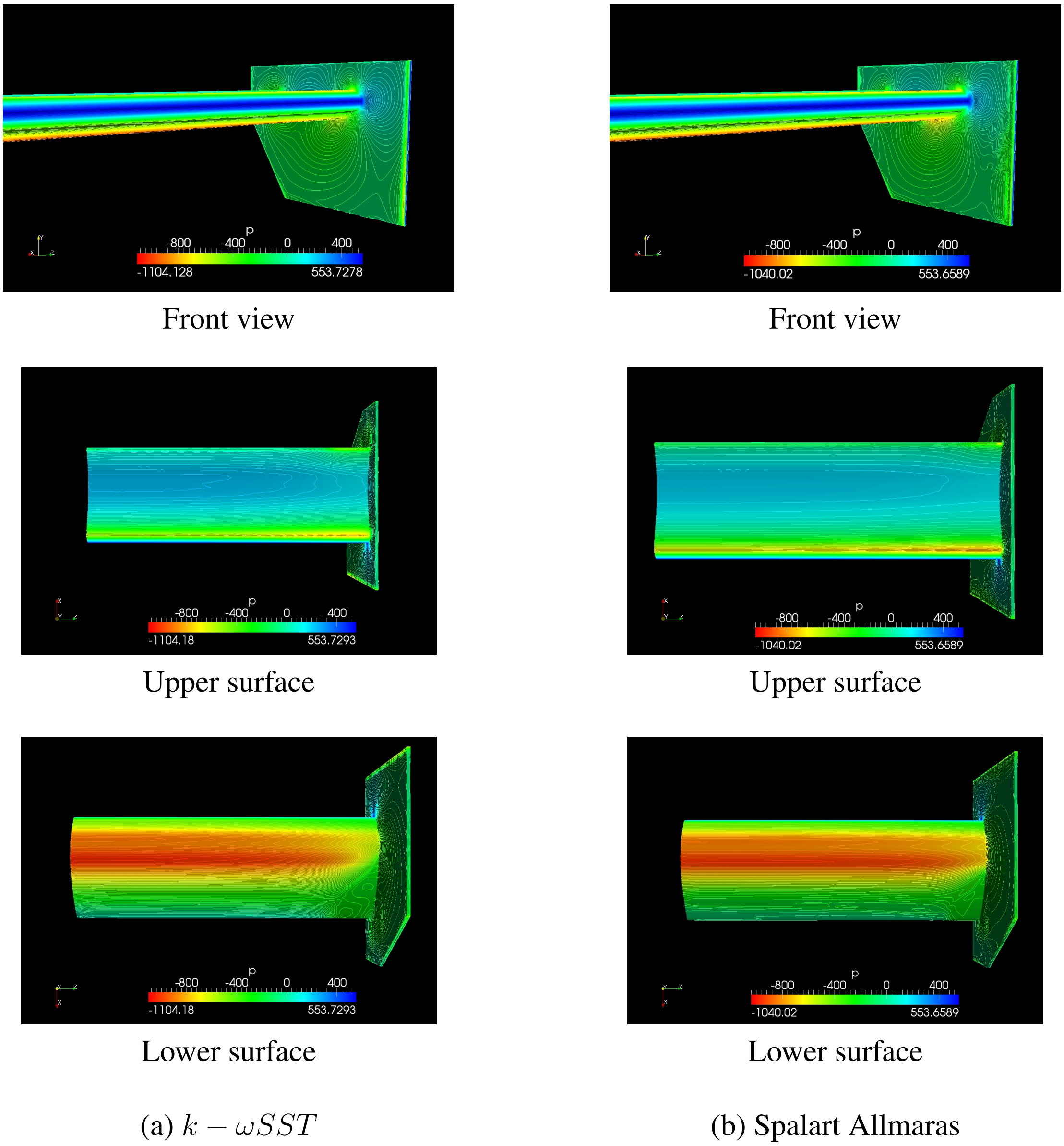

Figure 8: Computed pressure contours on the wing surface for $0°$ of incidence

Figure [9] shows the pressure contour for $15°$ of incidence. Here, a much lower pressure on the wing bottom is produced due the considerable velocity induced by the larger angle of attack. It seems that no much changes were produced in the pressure distribution at the upper surface, although comparing it with the former figure, the velocity at the trailing edge is much smaller. An additional effect of the larger angle of attack is the boundary layer separation (showed in dark green) located on the aft portion of the lower surface. It is the result of the abrupt rise in the pressure due to the strong fluid deceleration in the middle of the suction surface of the wing. This zone is characterized by flow recirculation and lost of aerodynamic pressure (negative pressure). Another important feature that must be pointed out is again the influence of the tip vortex. In this case, unlike the former case, it helps to prevent the boundary layer separation in the vicinity of the wing tip. The tip vortex helps to prevent the separation transferring part of its kinetic energy oncoming flow allowing it to keep attached to the surface for a little more distance. In this regard, the $k-\omega SST$ model predicted a bigger influence, meaning less separation than the Spalart Allmaras model, which translates in more lift and less drag.

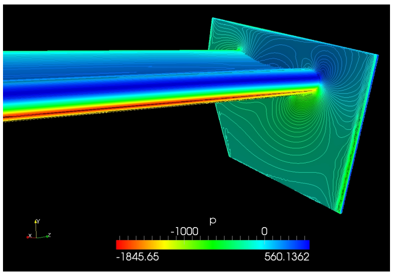

Isometric view

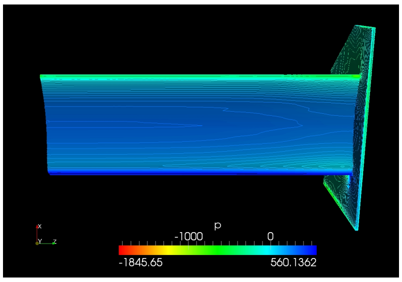

Upper surface

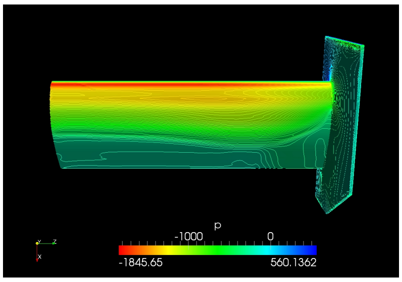

Lower surface

(a) $k-\omega SST$

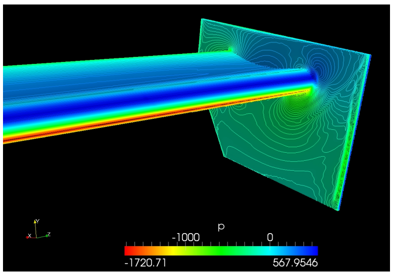

Isometric view

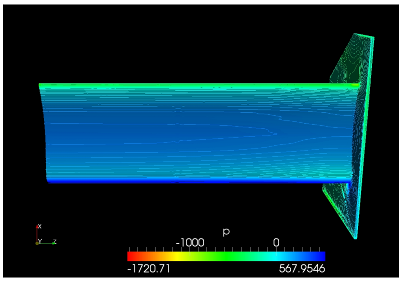

Upper surface

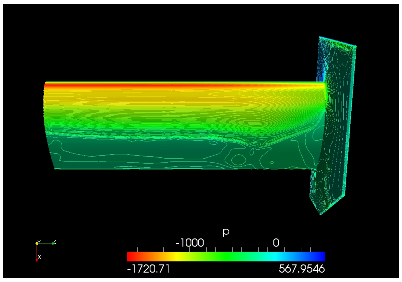

Lower surface

(b) Spalart Allmaras

Figure 9: Computed pressure contours on the wing surface for $15°$ of incidence

In order to clarify how the pressure varies along the wing in the streamwise direction, five planes along the wing spanwise direction were selected to plot the pressure coefficient versus the cord length. Figure [10] shows these plots for two angles of attack and both turbulence models.

For $0°$ of incidence, the pressure coefficient in the upper surface starts at the maximum value corresponding to the low speed at the foremost point. Then it drops and rises steeply in the excessively rounded vicinity of the leading edge. After passing this region it continues growing until the trailing edge neighborhood, then it drops again due to the extremely rounded form of the trailing edge. In similar way, the pressure in the lower surface starts dropping from the maximum value in the leading edge, but in this case it continues dropping almost to the middle of wing where the pressure starts growing until the trailing edge. From 80% of the wing span onwards, the effects of the wing tip vortex can be noticed in the decrease of the pressure distribution. The boundary layer separation can be easily distinguished, as it can be associated to constant pressure regions in the pressure distribution. Comparing the turbulence models, it can be observed that the $k - \omega SST$ model predicts a wider attached region on the suction surface even in the middle of the wing ($z/s = 0$). This behavior affects directly the overall lift value, but do not justify the discrepancy between the results predicted by both models, since the minimum pressure predicted by the Spalart Allmaras model is indeed higher compared to the pressure predicted by the $k - \omega SST$ model.

For $15°$ of incidence, the trend in the C_p distribution is totally different. The steep pressure drop in the leading edge is no longer seen, because the angle of incidence shifted the stagnation point to a higher position, avoiding the excessive acceleration in this part of the wing. The suction surface also presents a different distribution; here the maximum acceleration is reached very close to the leading edge, after which a greater adverse pressure region is observed. This increased adverse pressure region generates a premature separation of the boundary layer, which can be seen in Fig. [9] as a constant value region in the pressure distribution along the wing span.

Moreover, it can be observed a positive influence on the pressure distribution due to the tip vortex, since the pressure distribution in the planes near the tip ($z/s = 0.8$ and $z/s = 0.9$) present values of C_p even larger than those in the middle of the wing ($z/s = 0$). This influence remains positive only to the 80% of the wing span, where the tip vortex influence becomes negative promoting early boundary layer separation. Also, it is interesting to note the peaks in the pressure distribution just before the boundary separation. This feature is more pronounced in the Spalart Allmaras model, but it is present in both turbulence models. It seems that this pressure peak corresponds to a boundary layer reattachment after a recirculation tube which extents along the wing span.

Based on these results, one can observe that, while the wing tip vortex promotes boundary separation in the vicinity of the wing and end plate for both AoA, it helps delaying separation at a region located around 80% of the wingspan for higher AoA. The net effect is decrease in lift and increase in drag for low AoA, and increase in lift and decrease in drag for high AoA.

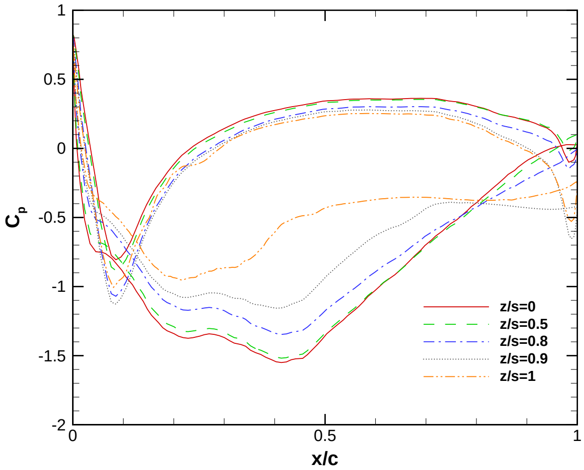

$k - \omega SST$ at $0°$ of incidence

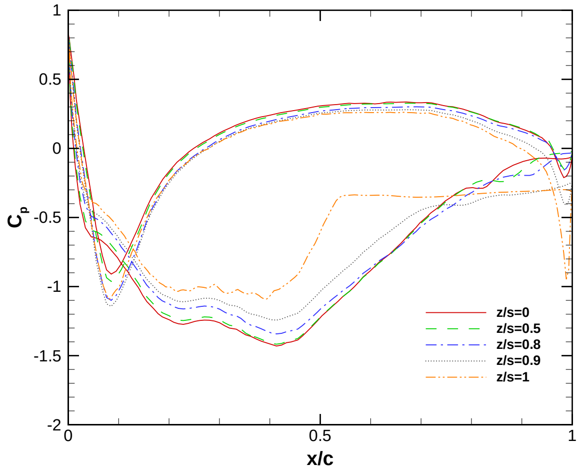

Spalart Allmaras at $0°$ of incidence

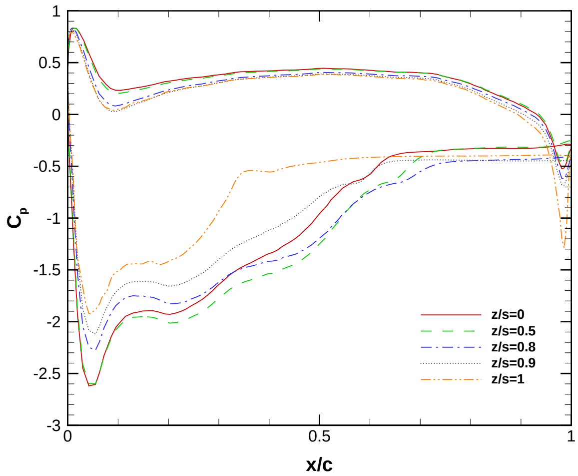

$k - \omega SST$ at $15°$ of incidence

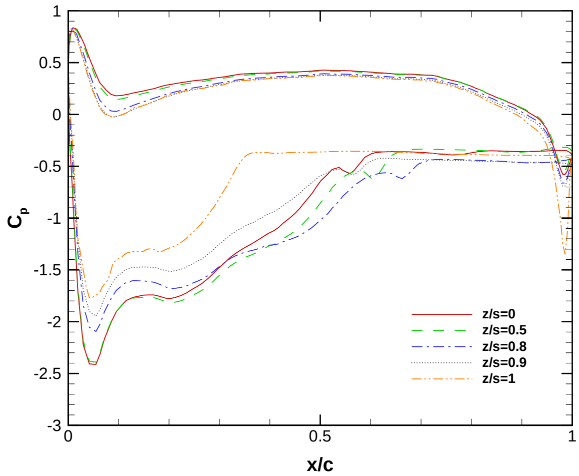

Spalart Allmaras at $15°$ of incidence

Figure 10: Chordwise surface pressure distributions at five cross sections

6.3 Flow Visualization

The origin and development of a tip vortex is shown in Fig.11. Here, the streamlines are distorted when they arrive to the wing, firstly at the top of the end plate. From that point onwards, the strong pressure difference between the upper and lower wing surfaces twists the streamlines towards the inner plane generating the first vortex. Meanwhile, at the rear part of the wing as well as at the lower part of the end plate, a strong negative pressure field along with the massive pressure difference between the upper and lower wing surfaces generate a central vortex behind the wing and a second vortex at the lower edge of the end plate. The stronger vortex alters the trajectory of the weaker ones while all of them travels upward. Further downstream, the three vortex merges in one, which continues growing in the streamwise direction.

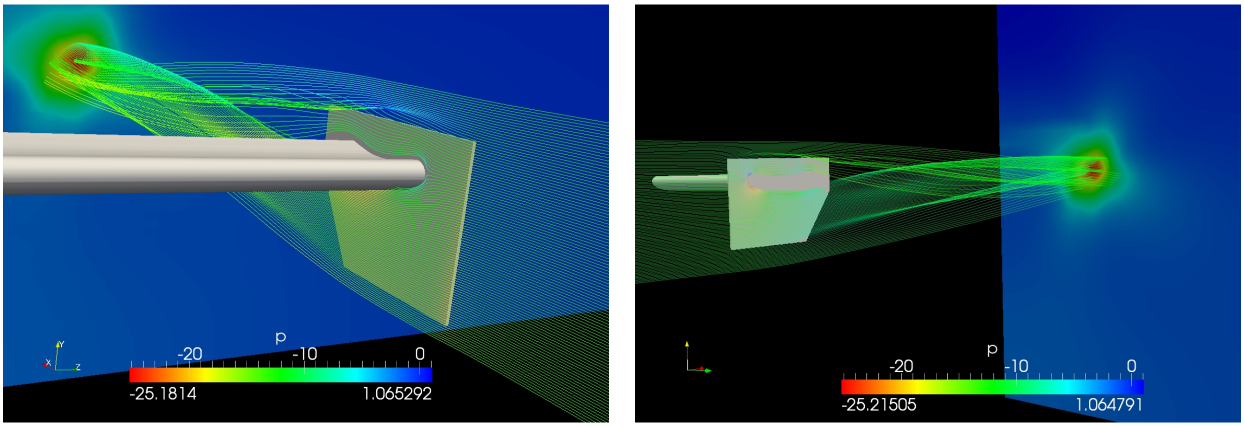

Figure 11: Streamlines showing the wing tip vortex development

Other very practical qualitative analysis of the flow behavior around the wing is one based on iso-contours of the coherence parameter Q. According to this criterion, the coherence of the vortices can be measured by the second invariant of velocity gradient.

Figure [12] depicts the formation of such structures. Apart from those previously observed, it is noted that a minor vortex is formed at the interior face of the end plate, which spins contouring the wing leading edge, for both angles of attack. This type of vortex, namely horseshoe vortex is produced by an upstream boundary layer on a surface that encounters an obstacle attached to that surface. The streamwise pressure gradients causes the approaching boundary layer to separate and form the horseshoe vortices, whereas pressure difference between the wing surfaces causes the near-wall flow to move around the obstacle Simpson (2001). Small coherent structures are also observed on the lower wing surface and on the interior face of the end plate. It seems that these structures are recirculation zones, related to local boundary layer separations. Since these structures are magnified in the case of the larger angle of incidence, its origin is attributed to the influence of the extensive pressure gradient at the suction zone.

7 CONCLUSIONS

A numerical simulation was carried out on the rear wing of the Formula Student car owned by PUC-Rio, using steady RANS equations along with two turbulence models. Moreover, an automatic mesh generation methodology provided by the OpenFOAM utility, snappyHexMesh, was evaluated regarding the compromise between the final mesh size and numerical errors. The following conclusions can be drawn from the results of this study.

- Not withstanding the lack of experimental data, the simulations accuracy (despite all its intrinsic uncertainties, like grid, turbulence models, etc.) seemed to be enough to capture the essential physics. In the near future, with the availability of experimental data it will be possible to know how reliable this methodology is, and whether it is ready to be employed for the analysis and development of aerodynamic devices.

- The three-dimensional behavior was found more intense near the wing tip, while in the middle of the wing the flow was found more uniform and almost two-dimensional. This behavior was noted to be intensified as the angle of attack increases, due to the intensification of the tip vortex energy and the increase of boundary-layer separation.

- The results showed that using elements with relatively high aspect ratio improved the results, decreasing the numerical diffusion in the near-wall region. More refinement was needed in the far field downstream of the wing in order to avoid numerical diffusion in the transitions from one level of refinement to the next level. This was also the case along the tip vortex path in order to better catch the gradients there.

- Generating the grid only by setting up its parameters decreased the total time needed to generate the grid compared with the time it would take to do it with a traditional method. Moreover, the total amount of elements in the unstructured grid was smaller due to the possibility of using an exponential local refinement. This would certainly translate to less labor hours and less processing time.

REFERENCES

Bienz C., Larsson T., and Ullbrand B. In front of the grid - cfd at sauber petronas f1 leading the aerodynamic development. *1st European Automotive CFD Conference*, 2003.

Galuol V. and Barber T. A study of an inverted wing with endplates in ground effect. *Australian Fluid Mechanics Conference* 16^{th}, 2007.

Genua E. *A CFD Investigation into Ground Effect Aerodynamics*. Master's Thesis, Delft University of Technology, 2009.

Larsson T., Sato T., and Ullbrand B. F1 supercomputing: Unlocking the power of cfd. Technical Report, SAUBER PETRONAS Engineering AG, 2005.

Peralta D. *Aerodynamic Study of a Racecar Rear Wing Using an Open-Source Computational Fluid Dynamics Software*. Master's Thesis, PUC-Rio, 2011.

Seibert W. and Lewis R. Motor sport drives cfd technology to a new level. Technical Report TN272, 2004.

Simpson R.L. Junction flows. *Annu. Rev. Fluid Mechanics*, 33:415–443, 2001.

Went J.F. *Computational Fluid Dynamics an Introduction*. Springer, third edition, 2009.

Zhang X., Zerihan J., Ruhrmann A., Deviese M., et al. Tip vortice generated by a wing in ground effect. *Proceedings of the 11th International Symposium on Applications of Laser Techniques to Fluid Mechanics*, 2002.

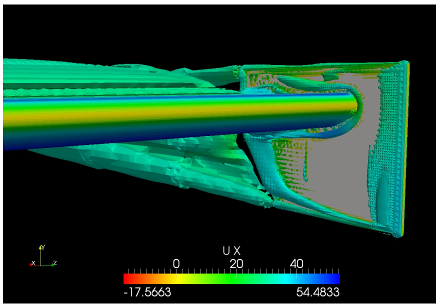

Front view $k - \omega SST$

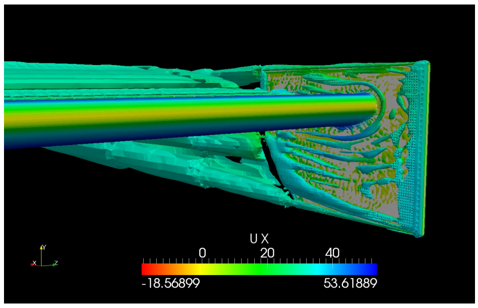

Front view Spalart Allmaras

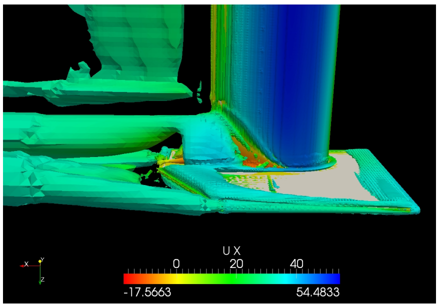

Lower surface view $k - \omega SST$

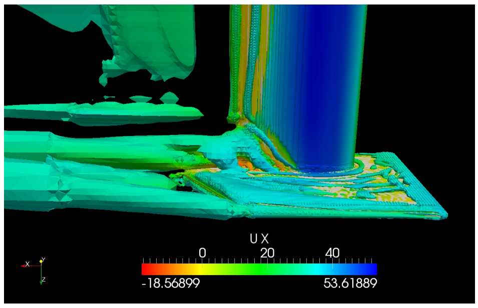

Lower surface view Spalart Allmaras

a) Wing at $0°$ of incidence

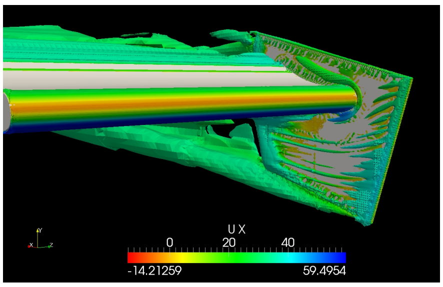

Front view $k - \omega SST$

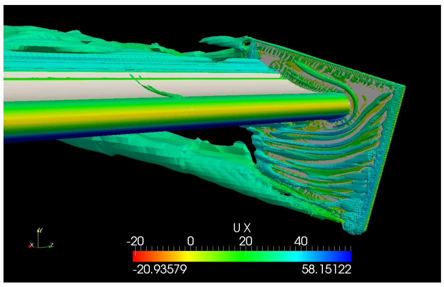

Front view Spalart Allmaras

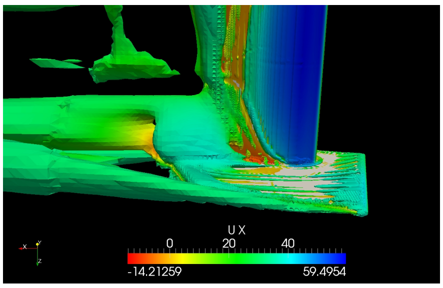

Lower surface view $k - \omega SST$

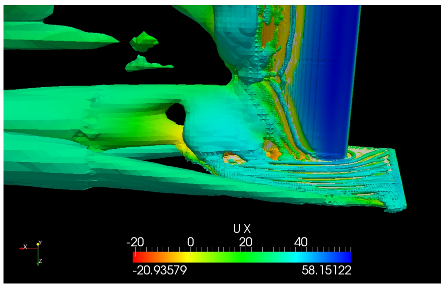

Lower surface view Spalart Allmaras

b) Wing at $15°$ of incidence

Figure 12: Coherent structures around the wing for $Q = 200$